Selective CO_2 Capture from Industrial Emissions and Biogas Using MUF-16: A Computational Study on Competitive Adsorption from Gas Mixtures

Elnaz Jangodaz[1,2] and Shane G. Telfer[1,2*]

[1] MacDiarmid Institute for Advanced Materials and Nanotechnology, School of Food Technology and Natural Sciences, Massey University, Palmerston North 4410, New Zealand.
[2] Captivate Technology Ltd, Palmerston North 4410, New Zealand.

Table of Contents

1. MUF-16 synthesis and PXRD

Small-scale synthesis: A mixture of $Co(OAc)_2 \cdot 4H_2O$ (0.1 mmol) and H_2aip (0.4 mmol), methanol (3.2 mL), and water (0.2 mL) was sonicated for 5 min in a 20 mL vial, which was then heated in a pre-heated oven at 85 °C for 3 h under autogenous pressure. The resulting powder was isolated by decanting off the mother liquor, washed with methanol several times, and then dried under vacuum oven at 130 °C overnight.

Larger-scale synthesis: A mixture of $Co(OAc)_2 \cdot 4H_2O$ (9.997 g, 40.136 mmol) and H_2aip (5-aminoisophthalic acid, 14.601 g, 80.602 mmol) and ethanol (100 mL) were refluxed in a 250 mL round-bottom flask overnight. The pink precipitate was filtered off while hot, successively washed with ethanol and water several times, and then dried under vacuum oven at 130 °C overnight. [1-3]

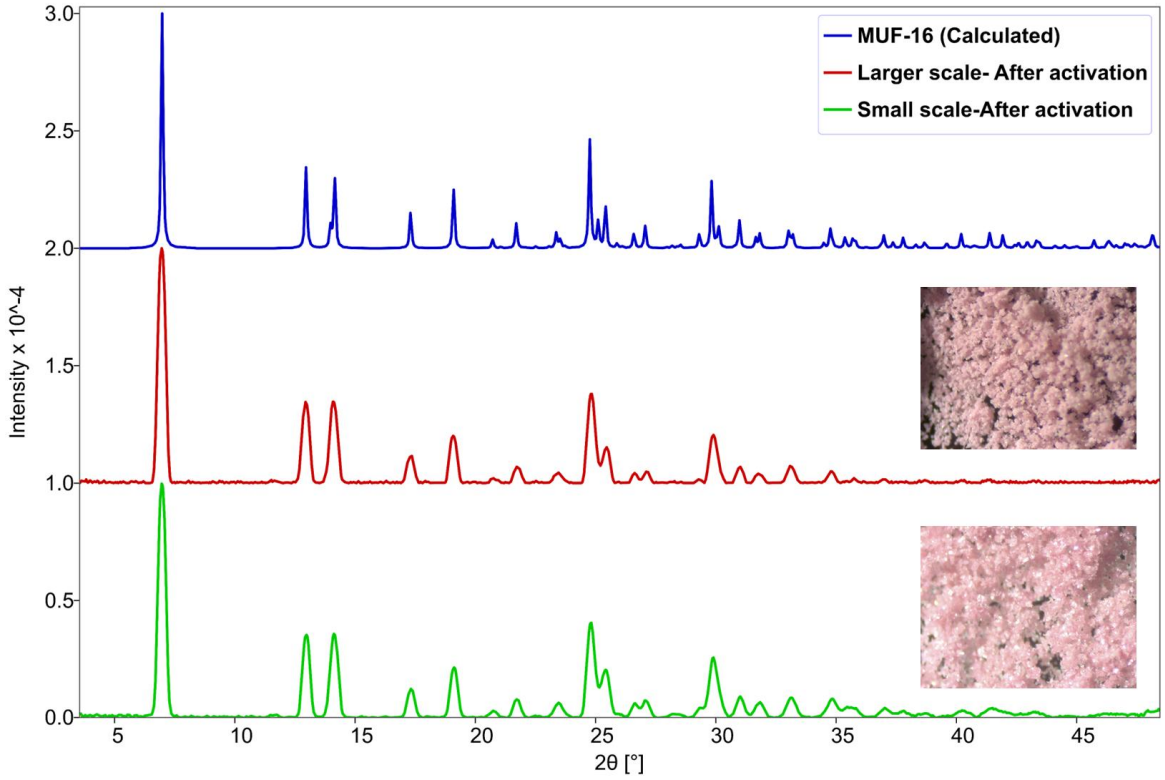

Figure S1 PXRD patterns of MUF-16 calculated from its SCXRD structure compared to MUF-16 synthesized by two different scales.

2. Details of RASPA simulation inputs

The simulation used 10000 cycles and 10000 initialization cycles for a 1 × 6 × 2 supercell of MUF-16. The framework geometry is considered to be rigid. The interactions between MUF-16 and adsorbates were represented by Lennard–Jones (LJ) parameters and electrostatic partial charges. The LJ parameters for MOF were derived from a combination of UFF and DREIDING force fields. A cutoff distance of 12 Å was employed, beyond which interactions were considered non-existent. The Charge Equilibration (QEq) method implemented in RASPA was used to calculate atomic charge. Different known force fields and molecular models were examined, and the best ones were identified based on their ability to achieve the closest match between CO_2 experimental and simulated results. For MUF-16, which has a relatively simple structure, all tested models

produced similar results. However, certain force fields, such as the "Generic MOFs" force field available in RASPA, tended to overestimate adsorption at low partial pressures. Certain models for the adsorbate underestimated the adsorption uptake. Since our goal is not to delve into the detailed identifying procedure, we focus on presenting the models that best describe the adsorption behaviour of MUF-16 and that show good agreement with experimental data.

Table S1 Lenard-Jones parameters of every framework atom type with a mixture of UFF and DREIDING force fields.[4]

Atom	σ (Å)	ε/k_B(K)	Force field
O	48.1581	3.03315	DREIDING
N	38.9492	3.26256	DREIDING
C	47.8562	3.47299	DREIDING
F	36.4834	3.0932	DREIDING
B	47.8058	3.58141	DREIDING
P	161.03	3.69723	DREIDING
S	173.107	3.59032	DREIDING
Cl	142.562	3.51932	DREIDING
Br	186.191	3.51905	DREIDING
H	7.64893	2.84642	DREIDING
Al	155.998	3.91105	DREIDING
Si	155.998	3.80414	DREIDING
Zn	62.3992	2.46155	UFF
Be	42.7736	2.44552	UFF
Cr	7.54829	2.69319	UFF
Fe	6.54185	2.5943	UFF
Mn	6.54185	2.63795	UFF
Cu	2.5161	3.11369	UFF
Co	7.04507	2.55866	UFF
Ga	208.836	3.90481	UFF
Ti	8.55473	2.8286	UFF
Sc	9.56117	2.93551	UFF
V	8.05151	2.80099	UFF
Ni	7.54829	2.52481	UFF
Zr	34.7221	2.78317	UFF
Mg	55.8574	2.69141	UFF
Ne	21.1352	2.88918	UFF
Ag	18.1159	2.80455	UFF
In	301.428	3.97608	UFF
Cd	114.734	2.53728	UFF
Sb	225.946	3.93777	UFF
I	170.57	4.01	-

Te	200.281	3.98232	UFF

Table S2 Molecular models of the adsorbates considered in this work.

Adsorbates	Geometry	Site	σ (Å)	ε/k_B(K)	q(e)	Reference
CO_2	dCO = 1.16 Å	C	2.80	27.0	0.70	5.6
	∠OCO = 180°	O	3.05	79.0	-0.35	
N_2	dNN = 1.1 Å	N	3.303	38.298	-0.405	7
		COM	-	-	0.810	
CH_4	United-atom model	CH_4	3.72	158.8	0	8
O_2	dOO = 1.2 Å	O	3.306	38.298	-0.112	7
		COM	-	-	0.224	
H_2	dHH = 0.74 Å	H	2.958	36.7	0.466	9
		COM	-	-	-0.932	
CO	dCO = 1.128 Å	C	3.636	16.141	-0.2424	10
		O	2.979	98.014	-0.2744	
		COM	-	-	0.5168	
SO_2	dSO = 1.43 Å	S	3.41	189.353	0.402	11
	∠OSO = 119.5°	O	3.198	58.725	-0.201	
NO_2	dNO = 1.2 Å	N	3.24	50.36	0.146	5,12,13
	∠ONO = 134.3°	O	2.93	62.51	-0.073	
NO	dNO = 1.15 Å	N	3.014	79.5	0.0288	5,14
		O	2.875	96.94	-0.0288	
H_2S	dSH = 1.34 Å	S	3.73	250	0.4	15
	∠HSH = 92°	H	0.98	3.9	0.25	
		COM	-	-	-0.9	

Table S3 Point charges for the MUF-16 obtained in RASPA using Charge Equilibration (QEq) method.

No.	Atom	Charge
1	Co	0.890712
2	O	-0.37579
3	O	-0.38256
4	O	-0.27655
5	O	-0.46761
6	H	0.31924
7	N	-0.28748
8	H	0.118452
9	H	0.120407
10	C	-0.05232
11	C	0.354999
12	C	-0.00167
13	H	0.061897
14	C	-0.08746
15	H	0.076733
16	C	0.117894
17	C	0.359719
18	C	-0.04651
19	C	-0.09347
20	H	0.096542

```
SimulationType                MonteCarlo
NumberOfCycles                10000
NumberOfInitializationCycles  10000
PrintEvery                    100
RestartFile                   no

Forcefield                    ForceField
UseChargesFromCIFFile         yes

Framework 0
FrameworkName MUF16
UnitCells 1 6 2
HeliumVoidFraction 0.156
ExternalTemperature 293.0
ExternalPressure  101325

Component 0 MoleculeName             CO2
            MoleculeDefinition       ExampleDefinitions
            TranslationProbability   0.5
            RotationProbability      0.5
            ReinsertionProbability   0.5
            SwapProbability          1.0
            CreateNumberOfMolecules  0
```

Figure S2 Example of a RASPA input file for isotherm prediction.

3. Physical-chemical properties of guest molecules

Table S4 Physicochemical properties of various gases.[2,16-18]

Gas molecule	Boiling point (K)	Kinetic diameter (Å)	Polarizability (Å^3)	Quadrupole moment× 10^{26} (esu cm^2)	Dipole moment ×10^{18} (esu cm^2)
CO_2	217	3.3	2.91	-4.3	0
N_2	77	3.64	1.74	-1.47	0
H_2	20	2.83-2.89	0.8	0.662	0
O_2	90	3.46	1.58	-0.39	0
CH_4	112	3.76	2.59	0	0
CO	82	3.69	1.95	-2.45	0.11
NO	121	3.49	1.7	0.62	0.16
NO_2	302	3.7	3.02	-	0.32
SO_2	262	3.6	3.72-4.28	-	1.63
H_2S	213	3.62	3.78-3.95	-	0.97

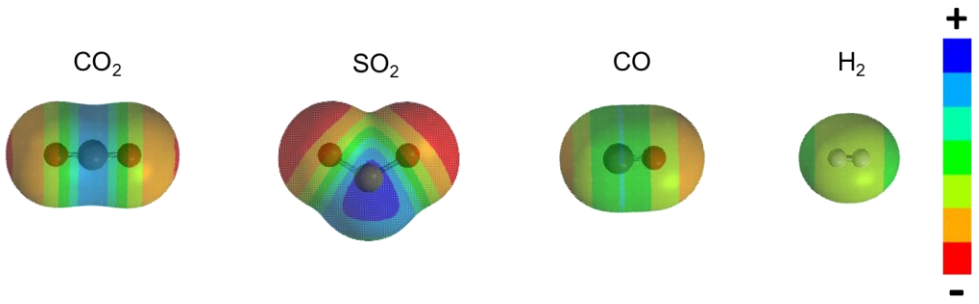

Figure S3 Electrostatic potential maps for CO_2, SO_2, CO, and H_2. These maps were calculated in Spartan with Hartree-Fock 6-311+G** calculations. Blue/green = positive; red/orange = negative.

4. Heat of adsorption calculation

To determine the isosteric heat of adsorption (Q_{st}),[19-21] experimental adsorption isotherms were collected at different temperatures then fitted to a virial equation of the form:

$$\ln P = \ln N + \frac{1}{T}\sum_{i=0}^{m} a_i N^i + \sum_{i=0}^{n} b_i N^i \qquad \text{S1}$$

where N is the amount of gas adsorbed at pressure P, and a and b are the virial coefficients. The integers m and n represent the number of coefficients required to adequately describe the isotherm. If the virial fit is satisfactory, the fitted parameters (a_0 to a_m) were then used to calculate the isosteric heat of adsorption (Q_{st}) using the following equation:

$$Q_{st} = -R\sum_{i=0}^{m} a_i N^i \qquad \text{S2}$$

where R is the universal gas constant 8.314 J/K/mol, N is the adsorbed amount. Q_{st} is a positive quantity and for an adsorption process the enthalpy of adsorption, ΔH_{ads}, has to be negative, therefore $\Delta H_{ads} = -Q_{st}$.

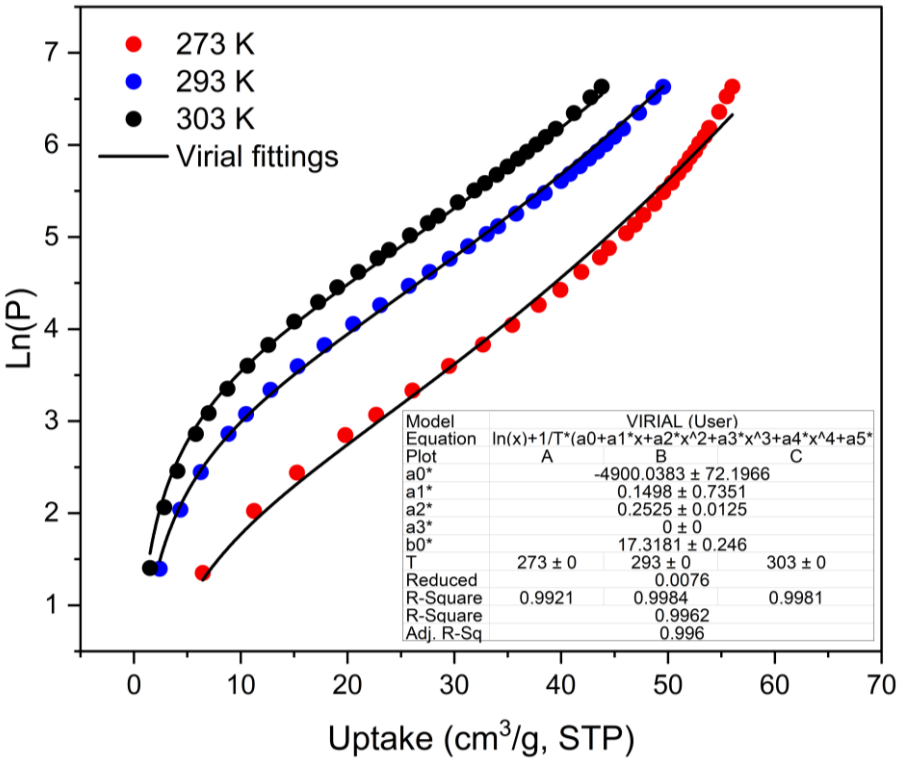

Figure S4 Virial equation fits for CO_2 adsorption isotherms of MUF-16.

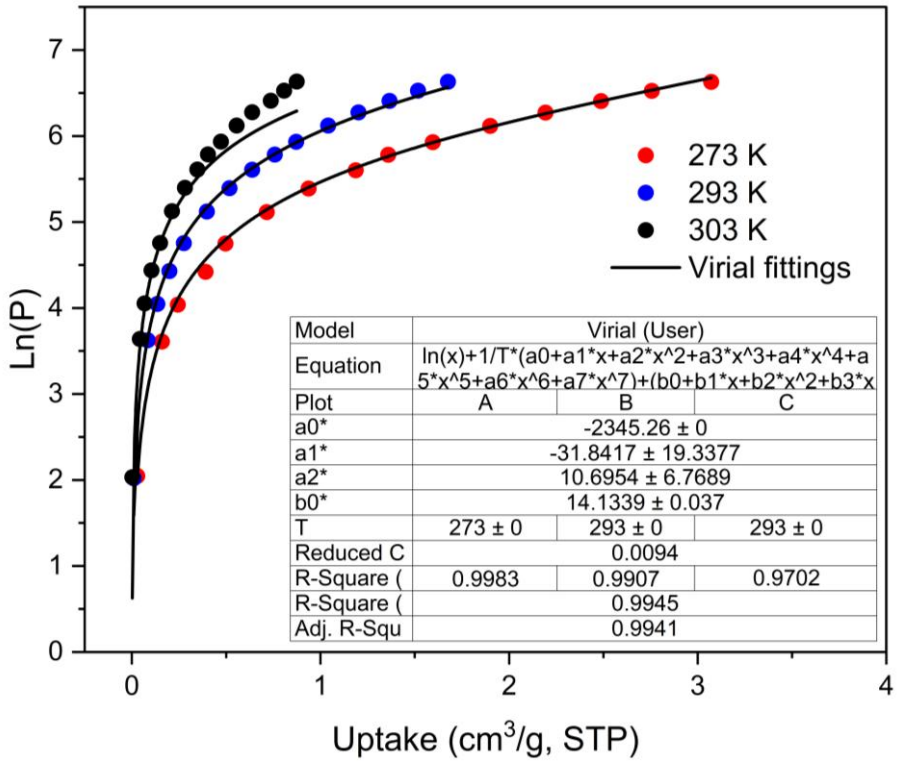

Figure S5 Virial equation fits for N_2 adsorption isotherms of MUF-16.

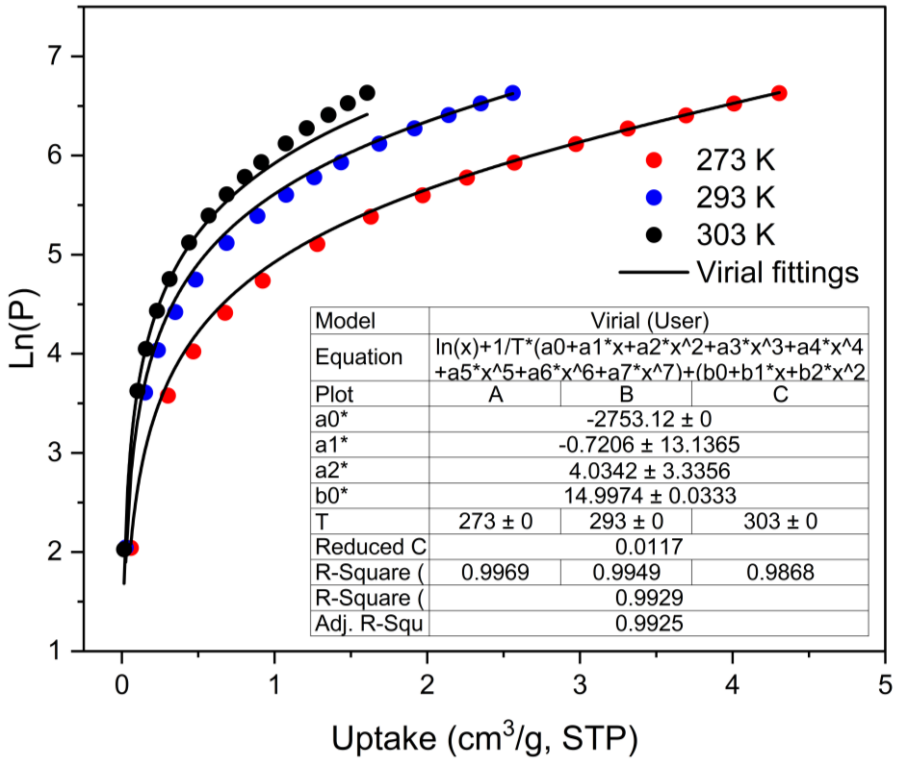

Figure S6 Virial equation fits for CH_4 adsorption isotherms of MUF-16.

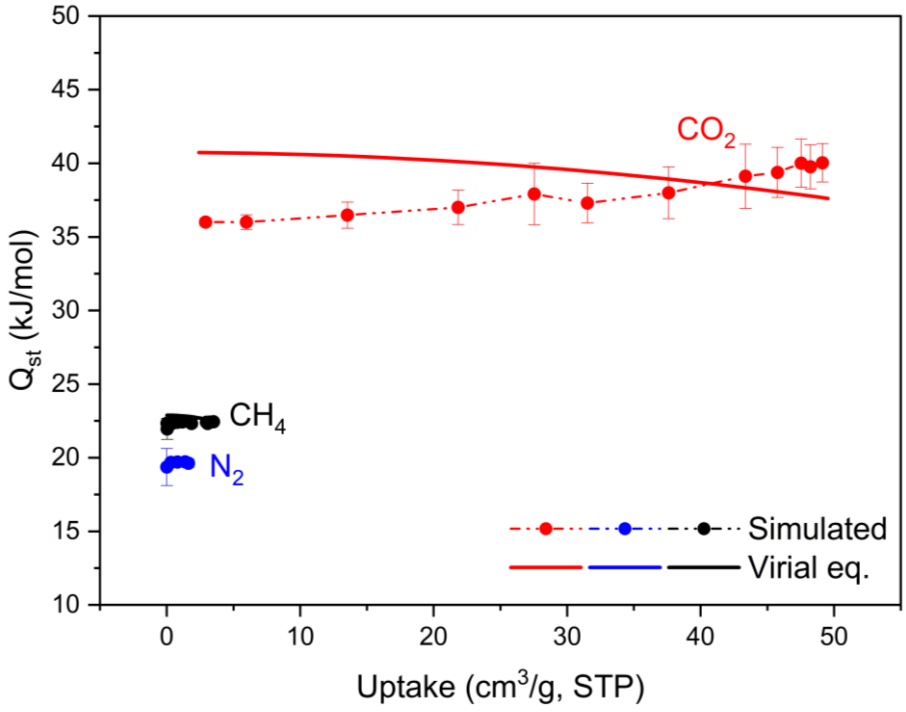

Figure S7 Isosteric heat of adsorption plotted as a function of uptake for the adsorption of CO_2, N_2, and CH_4 by MUF-16.

5. Experimental single gas adsorption isotherms

Gas adsorption isotherms were measured using a volumetric adsorption analyser (Quantachrome Autosorb-iQ2). High-purity gases (CO_2, N_2, CH_4, and He) were used as supplied by BOC Gases. Approximately 0.5 g of the as-synthesized sample was placed into a pre-dried, pre-weighed sample tube and heated at a rate of 5 °C/min to 130 °C under dynamic vacuum using a turbomolecular pump for 20 hours. After activation, accurate sample masses were determined using the degassed samples, following backfilling of the sample tubes with nitrogen. Surface area and pore volume were derived from the N_2 (77 K) adsorption isotherm using the BET model and total pore volume calculations performed with VersaWin software. Bath temperatures of 273 K, 293 K, and 303 K were precisely maintained using a recirculating temperature control system containing an ethylene glycol–water mixture. The low temperature (77 K) was achieved using a Dewar filled with liquid nitrogen.

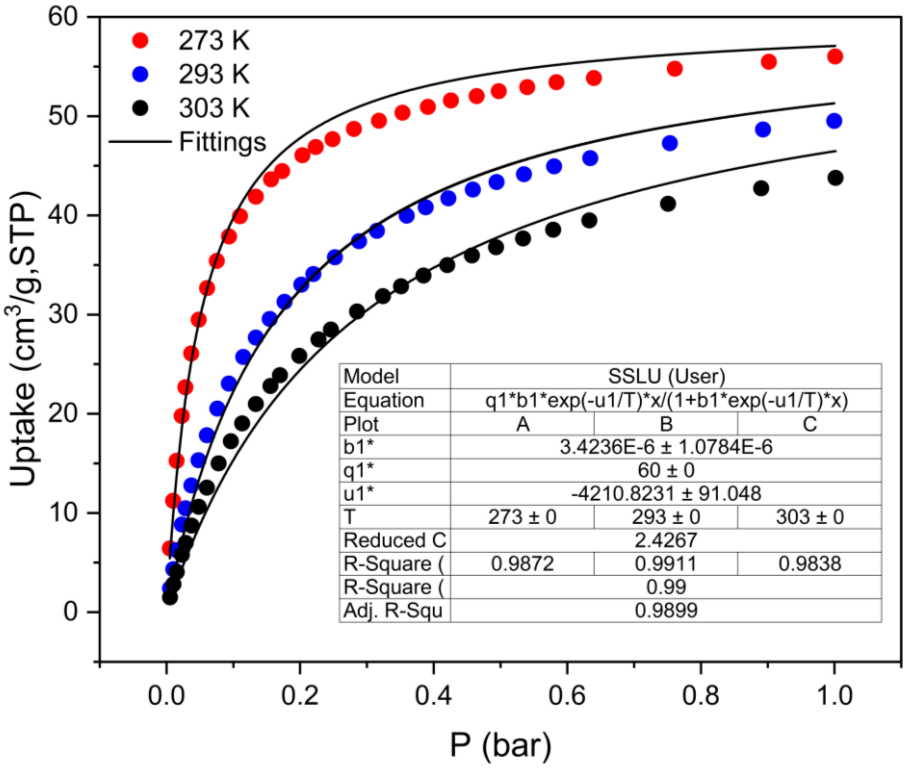

Figure S8 Single-site Langmuir fits of the experimental CO_2 isotherms on MUF-16.

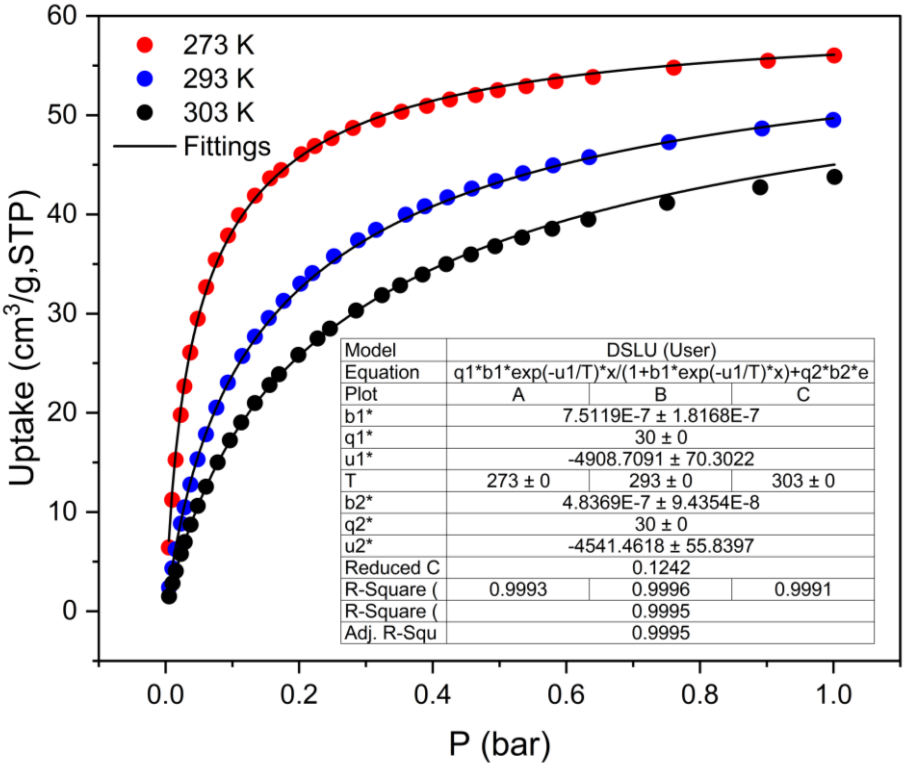

Model	DSLU (User)		
Equation	q1*b1*exp(-u1/T)*x/(1+b1*exp(-u1/T)*x)+q2*b2*e		
Plot	A	B	C
b1*	7.5119E-7 ± 1.8168E-7		
q1*	30 ± 0		
u1*	-4908.7091 ± 70.3022		
T	273 ± 0	293 ± 0	303 ± 0
b2*	4.8369E-7 ± 9.4354E-8		
q2*	30 ± 0		
u2*	-4541.4618 ± 55.8397		
Reduced C	0.1242		
R-Square (	0.9993	0.9996	0.9991
R-Square (	0.9995		
Adj. R-Squ	0.9995		

Figure S9 Dual-site Langmuir fits of the experimental CO_2 isotherms on MUF-16.

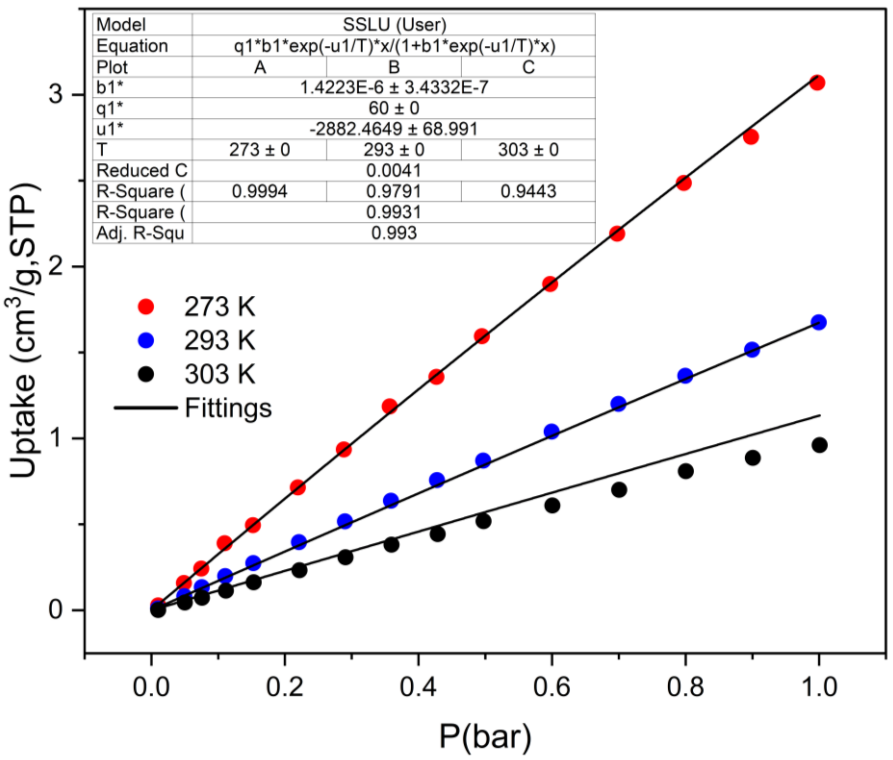

Model	SSLU (User)		
Equation	q1*b1*exp(-u1/T)*x/(1+b1*exp(-u1/T)*x)		
Plot	A	B	C
b1*	1.4223E-6 ± 3.4332E-7		
q1*	60 ± 0		
u1*	-2882.4649 ± 68.991		
T	273 ± 0	293 ± 0	303 ± 0
Reduced C	0.0041		
R-Square (	0.9994	0.9791	0.9443
R-Square (	0.9931		
Adj. R-Squ	0.993		

Figure S10 Single-site Langmuir fits of the experimental N_2 isotherms on MUF-16.

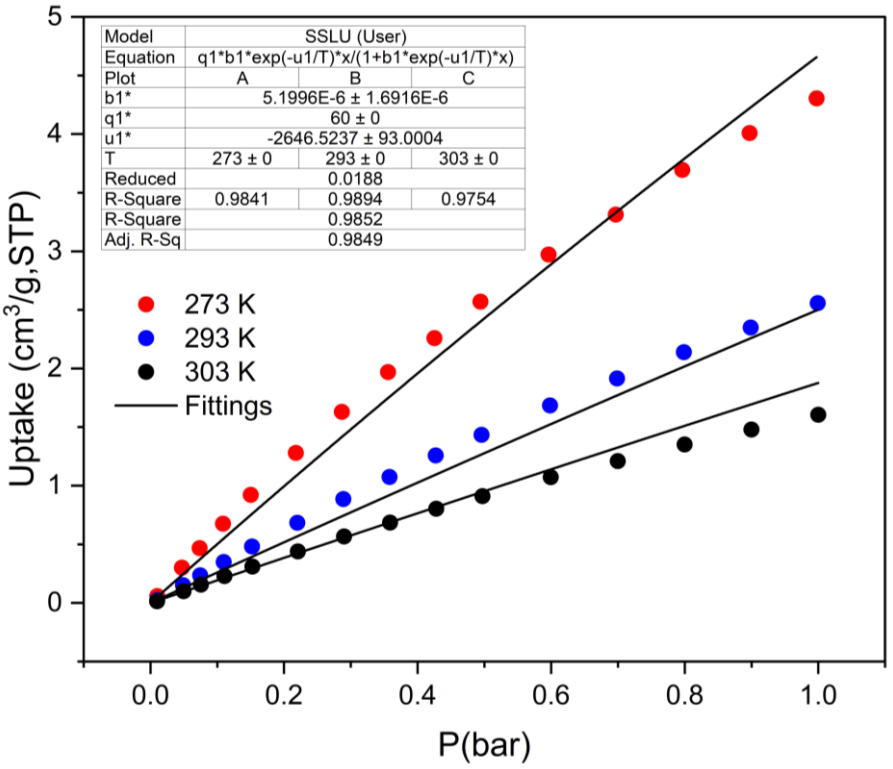

Figure S11 Single-site Langmuir fits of the experimental CH_4 isotherms on MUF-16.

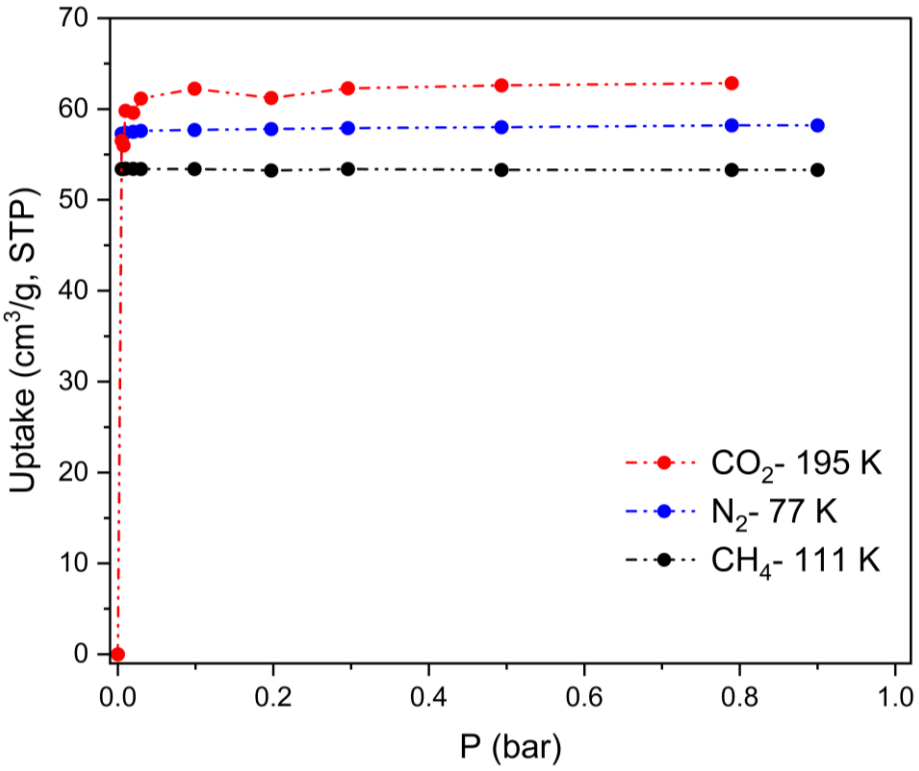

Figure S12 Simulated adsorption isotherms of CO_2, CH_4, and N_2 at their boiling points using RASPA.

6. BET calculation

Surface area and pore volume can be derived from the experimental N_2 (77 K) adsorption isotherm using the BET model and pore volume calculations performed with VersaWin software. When adsorption reaches saturation, the isotherm plateaus. At this point, the accessible pore volume of the material can be calculated by software. Also, a procedure proposed by Walton and Snurr[22] for selecting the appropriate pressure range for BET surface area determination was followed in this study:

1) The isotherm region where $v(1 - P/P_0)$ increases versusP/P_0, where v is the amount of N_2 adsorbed, was identified. Here, P/P_0 is the relative pressure, and P_0 is the condensation pressure of the adsorbent at the temperature of measurement.

2) Within this isotherm region, sequential data points that led to a positive intercept in the plot of $\frac{P/P_0}{v(1-P/P_0)}$ against P/P_0, were found. This plot yields a slope a, and a positive intercept b. The number of gas molecules adsorbed in the initial monolayer is $v_m = \frac{1}{a+b}$.

3) The BET surface area was then calculated according to the following equation:

$$S_{BET} = v_m(cm^3 g^{-1}) * \frac{1\ (mol)}{22400\ (cm^3)} * \sigma_0(\text{Å}^2) * N_A(mol^{-1}) * 10^{-20}\left(\frac{m^2}{\text{Å}^2}\right) \qquad \textbf{S3}$$

Where S_{BET} is the BET surface area (m^2/g), N_A is Avogadro's constant, and σ_0 is the cross-sectional area of a N_2 molecule, which is 16.2 Å^2.

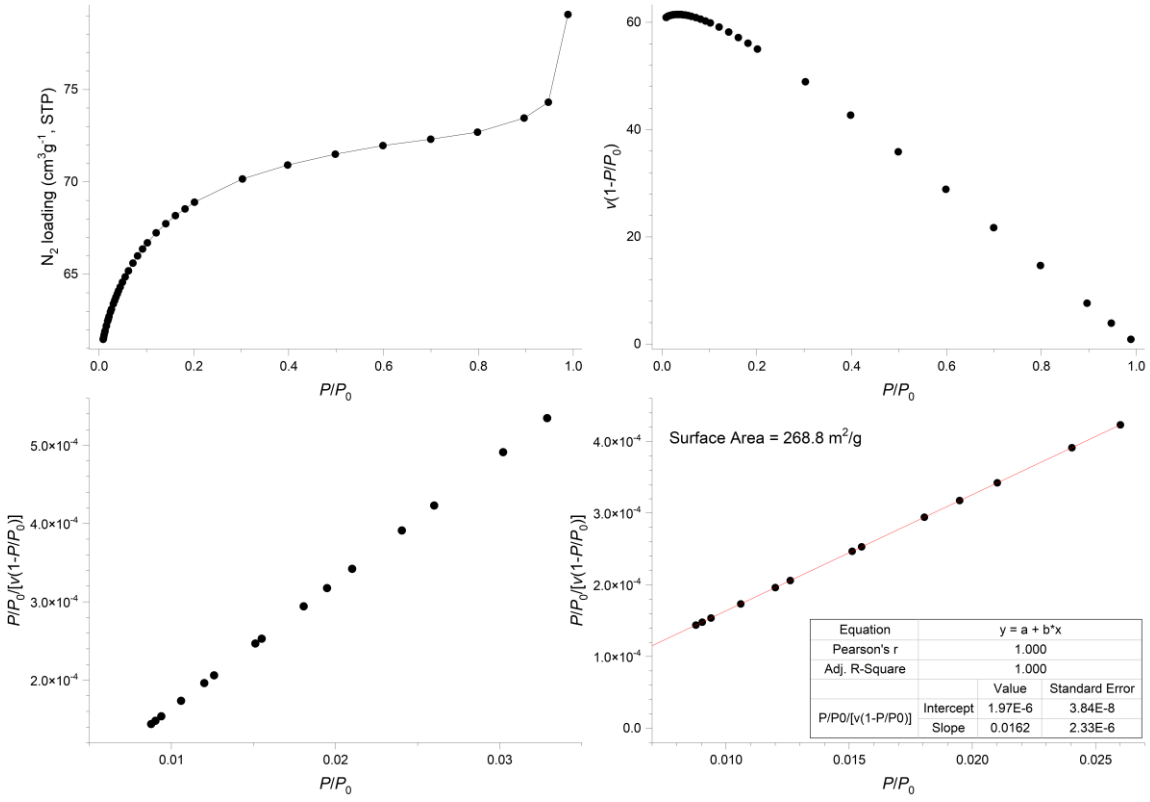

Figure S13 N_2 adsorption isotherm at 77 K and BET surface area plots for MUF-16.

7. IAST selectivity calculation

Selectivity represents the ratio of CO_2 uptake to the adsorption of another component (e.g., N_2) present in the flue gas stream or natural gas at a given gas composition.[23] S_{ads} is defined for separation of a binary mixture of species 1 and 2 by:

$$S_{ads} = \frac{q_1/q_2}{p_1/p_2} \qquad \textbf{S4}$$

Where the q_1 and q_2 represents the molar loading within the porous material that is in equilibrium with a bulk gas mixture with partial pressures p_1 and p_2. The values of q_1 and q_2 are obtained from multicomponent isothermal models. The S_{ads} values can be predicted from experimental adsorption isotherms of the individual single component gases by various methods. [23] The most common model for measuring selectivity is IAST (Ideal adsorbed solution theory), which use pure component isotherm data to predict adsorption behavior in gas mixtures.[24] Ideal Adsorbed Solution Theory (IAST) is a predictive model that does not need mixture data. It is widely used in gas purification and separation to estimate multicomponent adsorption equilibrium and selectivity using only single-component adsorption isotherms.[25]

Mixed gas adsorption isotherms and gas selectivity for different mixtures of CO_2/N_2 and CO_2/CH_4 were calculated at 293 K based on the ideal adsorbed solution theory (IAST) proposed by Myers and Prausnitz.[26] The IAST++ package[27] was used to perform the IAST calculations. Initially, single-component adsorption isotherms measured at different temperatures were fitted to either SSL or DSL models. The resulting fitting parameters were then used to carry out the IAST predictions.

8. Breakthrough experiment

In a typical breakthrough experiment, each activated sample (around 0.5 g) was placed in an adsorption column (6.4 mm in diameter × 11 cm in length) to form a fixed bed. The adsorbent was activated at 120 °C under high vacuum for 1 hour and then the column was left under vacuum while being cooled to 25 °C. The column was then purged under a 10 mLN/min flow of He gas for 10 min at 1 bar prior to the breakthrough experiment. A gas mixture 15/85 CO_2/N_2 was introduced to the column at 1 bar and 25 °C. A feed flowrate of 6 mLN/min was set. The operating pressure was controlled at 1 bar with a back-pressure regulator. The outlet composition was continuously monitored by the mass spectrometer until complete breakthrough was observed.

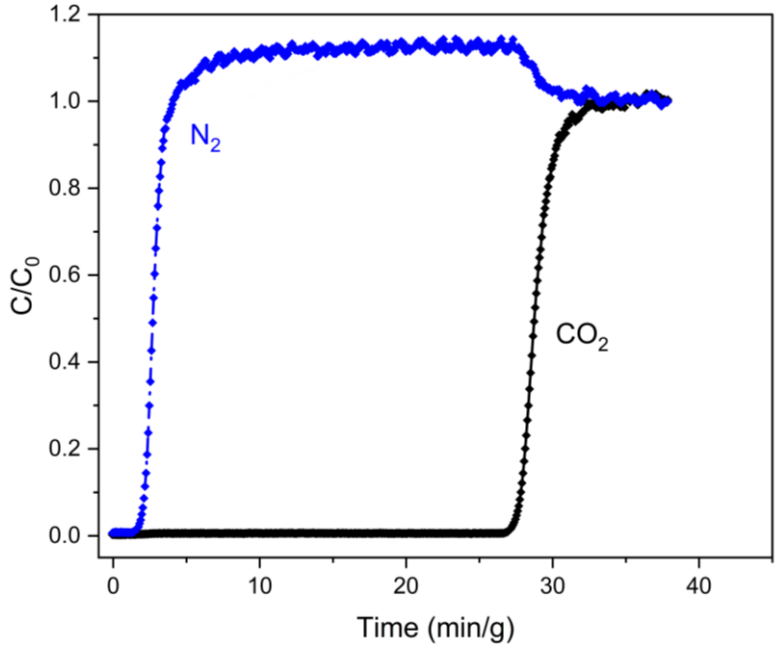

Figure S 14 Experimental breakthrough curves for a 15/85 CO_2/N_2 mixture, at 298 K and 1 bar in an adsorption column packed with MUF-16.

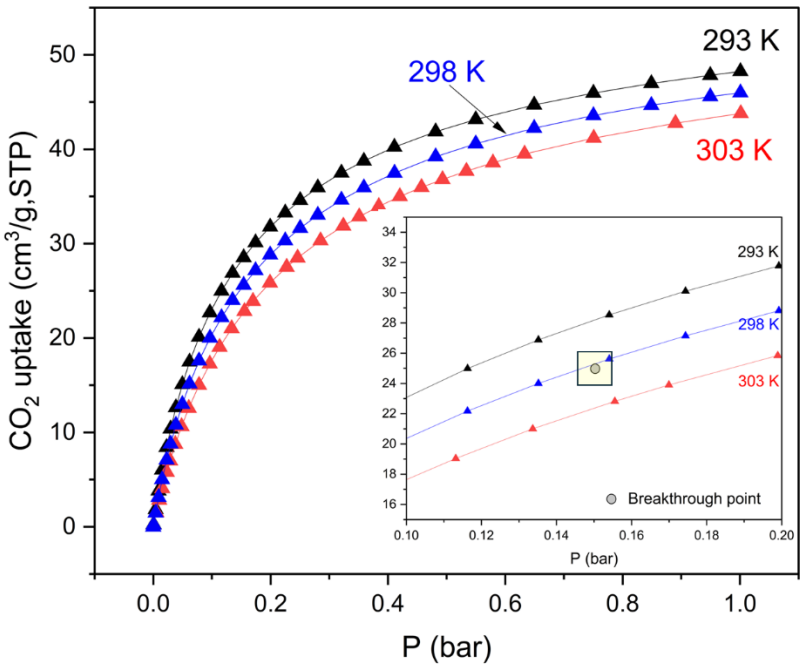

Figure S 15 Pure-component CO_2 adsorption isotherms for MUF-16 and the equilibrium CO_2 capacity (Gray circle) calculated from dynamic breakthrough experiments using a 15/85 CO_2/N_2 mixture at 298 K.

9. Single gas adsorption isotherm models

Unary gas isotherm fitting involves using mathematical models to represent the relationship between the amount of gas adsorbed onto a material and the pressure (or concentration) of that gas in contact with the material, at a

constant temperature. These mathematical equations are used to fit pure experimental data and predict adsorption behaviour. Common models include Langmuir, Freundlich, BET, and Sips.[28] Simple models, such as the Langmuir and Dual-Site Langmuir, are generally preferred for gas–solid adsorption isotherms as long as they provide a good fit to experimental data.

Langmuir adsorption model, originally developed to describe gas–solid adsorption, is widely used in process simulation due to its simplicity and effectiveness in fitting many experimental isotherms.[28] The Langmuir isotherm is a basic model for adsorption equilibrium, valid at both low and high pressures. It describes how adsorbate molecules cover the surface of a solid adsorbent depending on the gas' partial pressure or concentration at a fixed temperature.[29,30] The model assumes that:

- Molecules are adsorbed at discrete active sites on the surface.
- Each active site can adsorb only one molecule.
- The adsorbing surface is uniform.
- There is no interaction between adsorbed molecules.

From these perspectives, two forms of Langmuir model, SSL and DSL, are particularly suitable for Type I isotherm consider for our study (Figures S8-S11).
The SSL isotherm defines as below:

$$q^* = \frac{q_{sat,b} bp}{1 + bp} \quad \textbf{S5}$$

$$b = b_0 e^{\frac{-\Delta U_b}{RT}} \quad \textbf{S6}$$

The DSL isotherm takes the form:

$$q^* = \frac{q_{sat,b} bp}{1 + bp} + \frac{q_{sat,d} dp}{1 + dp} \quad \textbf{S7}$$

$$d = d_0 e^{\frac{-\Delta U_d}{RT}} \quad \textbf{S8}$$

Where q^* is the equilibrium loading of component, p is the pressure of the component, $q_{sat,b}$ and $q_{sat,d}$ show the saturation capacity of site b and d, ΔU_b and ΔU_d are the internal energy associated with sites b and d, respectively. The parameters b and d are the Langmuir constants corresponding to the adsorption sites b and d, which vary with temperature.

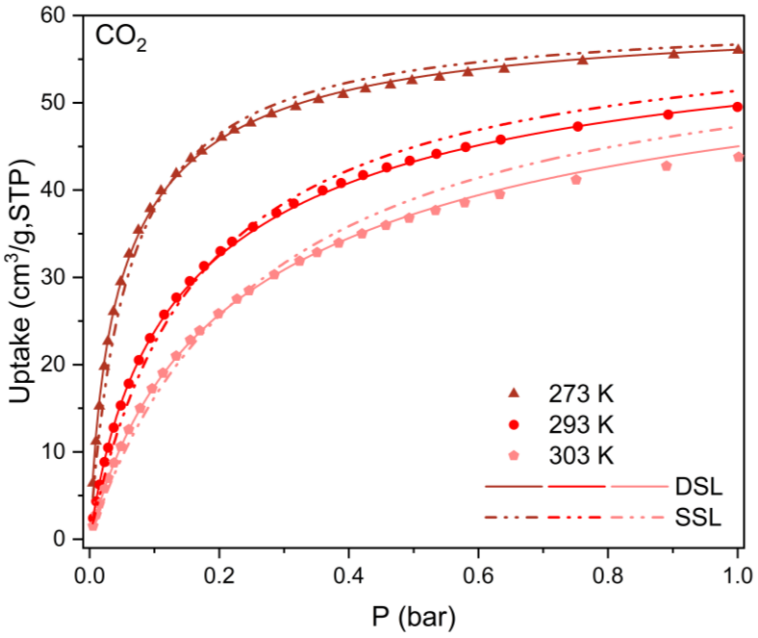

Figure S 16 Comparison of fitted SSL and DSL isotherm models for CO_2 at 273, 293, and 303 K. Markers represent experimental data, dashed lines represent SSL isotherms, and solid lines represent DSL isotherms.

10. Multicomponent adsorption isotherm models

In order to predict the sorption performance of MOFs toward the separation of binary mixed gases, the single-component adsorption isotherms were first fit to an appropriate model (Figures S8-S11). One of the earliest and most widely used models for multicomponent adsorption is the extended Langmuir model, also known as the multicomponent Langmuir model.[31] This model is a direct extension of the single-component Langmuir isotherm and provides an explicit formulation for mixture adsorption. Due to its simplicity and ease of implementation, the EL model is frequently employed in modelling multicomponent adsorption equilibria and simulating adsorptive separation processes.[32-34]

$$q_i^* = \frac{q_{sat,b,i} b_i p_i}{1 + \sum_{i=1}^{n} b_i p_i} \qquad \textbf{S9}$$

Where q_i^* is the equilibrium loading of component i, p_i is the pressure of the component i, $q_{sat,b,i}$ and $q_{sat,d,i}$ show the saturation capacity of site b and d for the component i, respectively, i denotes the component, n is the total number of components.

The dual-site form of the extended Langmuir (DSL) model is expressed as:

$$q_i^* = \frac{q_{sat,b,i} b_i p_i}{1 + \sum_{i=1}^{n} b_i p_i} + \frac{q_{sat,d,i} d_i p_i}{1 + \sum_{i=1}^{n} d_i p_i} \qquad \textbf{S10}$$

Here, b and d are Langmuir constants corresponding to the adsorption sites b and d, which are related to the adsorption equilibrium constant and the adsorption energy based on Eqs. S6 and S8; other descriptions are similar to Eq. S9.

Table S5 Fitting parameters used for IAST model and four binary adsorption approaches.

Parameter	EL			PP		
	CO_2	N_2	CH_4	CO_2	N_2	CH_4
$q_{sat,b}$ (cm^3/g, STP)	60	60	60	30	60	60
b_0 (1/bar)	3.424×10^{-6}	1.422×10^{-6}	5.199×10^{-6}	7.512×10^{-7}	1.422×10^{-6}	5.199×10^{-6}
ΔU_b (kJ/mol)	-35.01	-23.96	-22.00	-40.81	-23.96	-22.00
$q_{sat,d}$ (cm^3/g, STP)	-	-	-	30	-	-
d_0(1/bar)	-	-	-	4.837×10^{-7}	-	-
ΔU_d (kJ/mol)	-	-	-	-37.76	-	-

Continued

Parameter	PN			EES and IAST		
	CO_2	N_2	CH_4	CO_2	N_2	CH_4
$q_{sat,b}$ (cm^3/g, STP)	30	-	-	30	30	30
b_0 (1/bar)	7.512×10^{-7}	-	-	7.512×10^{-7}	1.422×10^{-6}	5.199×10^{-6}
ΔU_b (kJ/mol)	-40.81	-	-	-40.81	-23.96	-22.00
$q_{sat,d}$ (cm^3/g, STP)	30	60	60	30	30	30
d_0(1/bar)	4.837×10^{-7}	1.422×10^{-6}	5.199×10^{-6}	4.837×10^{-7}	1.422×10^{-6}	5.199×10^{-6}
ΔU_d (kJ/mol)	-37.76	-23.96	-22.00	-37.76	-23.96	-22.00

References

1. Qazvini, O. T.; Telfer, S. G., MUF-16: A Robust Metal–Organic Framework for Pre- and Post-Combustion Carbon Dioxide Capture. *ACS Appl. Mater. Interfaces* **2021,** *13* (10), 12141-12148.
2. Qazvini, O. T.; Babarao, R.; Telfer, S. G., Selective capture of carbon dioxide from hydrocarbons using a metal-organic framework. *Nat. Commun.* **2021,** *12* (1), 197.
3. Taheri Qazvini, O. Metal-organic frameworks for selective gas separation : a thesis presented in partial fulfilment of the requirements of the degree of Doctor of Philosophy in Chemistry at Massey University, Manawatū, New Zealand. Doctoral, *Massey University*, **2019**.
4. Dubbeldam, D.; Sofía, C.; E., E. D.; and Snurr, R. Q., RASPA: molecular simulation software for adsorption and diffusion in flexible nanoporous materials. *Mol. Simul.* **2016,** *42* (2), 81-101.
5. Sun, W.; Lin, L.-C.; Peng, X.; Smit, B., Computational screening of porous metal-organic frameworks and zeolites for the removal of SO_2 and NO_x from flue gases. *AIChE J.* **2014,** *60* (6), 2314-2323.
6. Li, Z.; Liao, F.; Jiang, F.; Liu, B.; Ban, S.; Chen, G.; Sun, C.; Xiao, P.; Sun, Y., Capture of H_2S and SO_2 from trace sulfur containing gas mixture by functionalized UiO-66(Zr) materials: A molecular simulation study. *Fluid Phase Equilib.* **2016,** *427*, 259-267.
7. Martín-Calvo, A.; García-Pérez, E.; García-Sánchez, A.; Bueno-Pérez, R.; Hamad, S.; Calero, S., Effect of air humidity on the removal of carbon tetrachloride from air using Cu–BTC metal–organic framework. *Phys. Chem. Chem. Phys.* **2011,** *13* (23), 11165-11174.
8. Martin, M. G.; Thompson, A. P.; Nenoff, T. M., Effect of pressure, membrane thickness, and placement of control volumes on the flux of methane through thin silicalite membranes: A dual control volume grand canonical molecular dynamics study. *J. Chem. Phys.* **2001,** *114* (16), 7174-7181.
9. Lithoxoos, G. P.; Labropoulos, A.; Peristeras, L. D.; Kanellopoulos, N.; Samios, J.; Economou, I. G., Adsorption of N_2, CH_4, CO and CO_2 gases in single walled carbon nanotubes: A combined experimental and Monte Carlo molecular simulation study. *J. Supercrit. Fluids* **2010,** *55* (2), 510-523.
10. Martín-Calvo, A.; Lahoz-Martín, F. D.; Calero, S., Understanding Carbon Monoxide Capture Using Metal–Organic Frameworks. *J. Phys. Chem. C* **2012,** *116* (11), 6655-6663.
11. Matito-Martos, I.; Martin-Calvo, A.; Gutiérrez-Sevillano, J. J.; Haranczyk, M.; Doblare, M.; Parra, J. B.; Ania, C. O.; Calero, S., Zeolite screening for the separation of gas mixtures containing SO_2, CO_2 and CO. *Phys. Chem. Chem. Phys.* **2014,** *16* (37), 19884-19893.
12. Matito-Martos, I.; Rahbari, A.; Martin-Calvo, A.; Dubbeldam, D.; Vlugt, T. J. H.; Calero, S., Adsorption equilibrium of nitrogen dioxide in porous materials. *Phys. Chem. Chem. Phys.* **2018,** *20* (6), 4189-4199.
13. Bourasseau, E.; Lachet, V.; Desbiens, N.; Maillet, J. B.; Teuler, J. M.; Ungerer, P., Thermodynamic behavior of the CO_2 + NO_2/N_2O_4 mixture: a Monte Carlo simulation study. *J. Phys. Chem. B* **2008,** *112* (49), 15783-92.

14. Zhou, Z.; Todd, B. D.; Travis, K. P.; Sadus, R. J., A molecular dynamics study of nitric oxide in water: Diffusion and structure. *J. Chem. Phys.* **2005,** *123* (5), 054505.
15. Gutiérrez-Sevillano, J. J.; Martín-Calvo, A.; Dubbeldam, D.; Calero, S.; Hamad, S., Adsorption of hydrogen sulphide on Metal-Organic Frameworks. *RSC Adv.* **2013,** *3* (34), 14737-14749.
16. Li, J.-R.; Kuppler, R. J.; Zhou, H.-C., Selective gas adsorption and separation in metal–organic frameworks. *Chem. Soc. Rev.* **2009**, *38* (5), 1477-1504.
17. Woodall, J.; Agúndez, M.; Markwick-Kemper, A. J.; Millar, T. J., The UMIST database for astrochemistry 2006*. *A&A* **2007**, *466* (3), 1197-1204.
18. Eguchi, R.; Uchida, S.; Mizuno, N., Inverse and High CO_2/C_2H_2 Sorption Selectivity in Flexible Organic–Inorganic Ionic Crystals. *Angew. Chem. Int. Ed.* **2012**, *51* (7), 1635-1639.
19. Nuhnen, A.; Janiak, C., A practical guide to calculate the isosteric heat/enthalpy of adsorption via adsorption isotherms in metal–organic frameworks, MOFs. *Dalton Trans.* **2020**, *49* (30), 10295-10307.
20. Moreno-Piraján, J. C.; Giraldo, L., Heat of Adsorption: A Comparative Study between the Experimental Determination and Theoretical Models Using the System CH4-MOFs. *J. Chem. Eng. Data* **2020**, *65* (6), 3130-3145.
21. Sircar, S.; Cao, D. V., Heat of Adsorption. *Chem. Eng. Technol.* **2002**, *25* (10), 945-948.
22. Walton, K. S.; Snurr, R. Q., Applicability of the BET Method for Determining Surface Areas of Microporous Metal−Organic Frameworks. *J. Am. Chem. Soc.* **2007**, *129* (27), 8552-8556.
23. Hu, Z.; Wang, Y.; Shah, B. B.; Zhao, D., CO_2 Capture in Metal–Organic Framework Adsorbents: An Engineering Perspective. *Adv. Sustain. Syst.* **2019**, *3* (1), 1800080.
24. Acharya, A.; Jeppu, G.; Raju Girish, C.; Prabhu, B., Development of a Multicomponent Adsorption Isotherm Equation and Its Validation by Modeling. *Langmuir* **2023**, *39* (49), 17862-17878.
25. Ismail, M.; Bustam, M. A.; Kari, N. E.; Yeong, Y. F., Ideal Adsorbed Solution Theory (IAST) of Carbon Dioxide and Methane Adsorption Using Magnesium Gallate Metal-Organic Framework (Mg-gallate). In *Molecules*, **2023**; Vol. 28.
26. Myers, A. L.; Prausnitz, J. M., Thermodynamics of mixed-gas adsorption. *AICHE J.* **1965**, *11* (1), 121-127.
27. Lee, S.; Lee, J. H.; Kim, J., User-friendly graphical user interface software for ideal adsorbed solution theory calculations. *Korean J. Chem. Eng.* **2018**, *35* (1), 214-221.
28. Ayawei, N.; Ebelegi, A. N.; Wankasi, D., Modelling and Interpretation of Adsorption Isotherms. *J. Chem.* **2017**, *2017* (1), 3039817.
29. Ye, W.; Pan, Y.; He, L.; Chen, B.; Liu, J.; Gao, J.; Wang, Y.; Yang, Y., Chapter 3 - Design with modeling techniques. In *Industrial Ventilation Design Guidebook (Second Edition)*, Goodfellow, H. D., Wang, Y. Eds.; Academic Press, **2021**; 109-183.
30. Langmuir, I., The adsorption of gases on plane surfaces of glass, mica and platinum. *J. Am. Chem. Soc.* **1918**, *40* (9), 1361-1403.

31. Van Assche, T. R. C.; Baron, G. V.; Denayer, J. F. M., An explicit multicomponent adsorption isotherm model: accounting for the size-effect for components with Langmuir adsorption behavior. *Adsorption* **2018**, *24* (6), 517-530.
32. Gomez, L. F.; Zacharia, R.; Bénard, P.; Chahine, R., Multicomponent adsorption of biogas compositions containing CO_2, CH_4 and N_2 on Maxsorb and Cu-BTC using extended Langmuir and Doong–Yang models. *Adsorption* **2015**, *21* (5), 433-443.
33. Moura, P. A. S.; Bezerra, D. P.; Vilarrasa-Garcia, E.; Bastos-Neto, M.; Azevedo, D. C. S., Adsorption equilibria of CO_2 and CH_4 in cation-exchanged zeolites 13X. *Adsorption* **2016**, *22* (1), 71-80.
34. Silva, J. A. C.; Ferreira, A.; Mendes, P. A. P.; Cunha, A. F.; Gleichmann, K.; Rodrigues, A. E., Adsorption Equilibrium and Dynamics of Fixed Bed Adsorption of CH_4/N_2 in Binderless Beads of 5A Zeolite. *Ind. Eng. Chem. Res.* **2015**, *54* (24), 6390-6399.